



Article

# Ag Nanoparticle-Decorated Cu<sub>2</sub>S Nanosheets for Surface Enhanced Raman Spectroscopy Detection and Photocatalytic Applications

Osama Nasr<sup>1</sup>, Jian-Ru Jiang<sup>2</sup>, Wen-Shuo Chuang<sup>1</sup>, Sheng-Wei Lee<sup>2,\*</sup> and Chih-Yen Chen<sup>1,\*</sup>

<sup>1</sup> Department of Materials and Optoelectronic Science, National Sun Yat-Sen University, Kaohsiung 804201, Taiwan; osamanasr@nssysu.edu.tw (O.N.); egg03@mail.mirdc.org.tw (W.-S.C.)

<sup>2</sup> Institute of Materials Science and Engineering, National Central University, Taoyuan 320317, Taiwan; icq200148@gmail.com

\* Correspondence: swlee@g.ncu.edu.tw (S.-W.L.); cychen@mail.nssysu.edu.tw (C.-Y.C.)

**Abstract:** In this article, we demonstrate a facile, rapid, and practical approach to growing high-quality Cu<sub>2</sub>S nanosheets decorated with Ag nanoparticles (NPs) through the galvanic reduction method. The Ag/Cu<sub>2</sub>S nanosheets were efficiently applied to the surface-enhanced Raman scattering (SERS) and photocatalytic degradation applications. The photodegradation of RhB dye with the Ag/Cu<sub>2</sub>S nanosheets composites occurred at a rate of 2.9 times faster than that observed with the undecorated Cu<sub>2</sub>S nanosheets. Furthermore, the Ag/Cu<sub>2</sub>S nanosheets displayed highly sensitive SERS detection of organic pollutant (R6G) as low as 10<sup>-9</sup> M. The reproducibility experiments indicated that the Ag/Cu<sub>2</sub>S nanosheets composites could be used for dual functionality in a new generation of outstandingly sensitive SERS probes for detection and stable photocatalysts.

**Keywords:** Cu<sub>2</sub>S nanosheets; Ag nanoparticles; SERS probes; photodegradation; photocatalysts



**Citation:** Nasr, O.; Jiang, J.-R.; Chuang, W.-S.; Lee, S.-W.; Chen, C.-Y. Ag Nanoparticle-Decorated Cu<sub>2</sub>S Nanosheets for Surface Enhanced Raman Spectroscopy Detection and Photocatalytic Applications. *Nanomaterials* **2021**, *11*, 2508. <https://doi.org/10.3390/nano11102508>

Academic Editor: Tsung-Shine Ko

Received: 5 August 2021

Accepted: 22 September 2021

Published: 26 September 2021

**Publisher's Note:** MDPI stays neutral with regard to jurisdictional claims in published maps and institutional affiliations.



**Copyright:** © 2021 by the authors. Licensee MDPI, Basel, Switzerland. This article is an open access article distributed under the terms and conditions of the Creative Commons Attribution (CC BY) license (<https://creativecommons.org/licenses/by/4.0/>).

## 1. Introduction

Nanostructured metal chalcogenides have been widely studied for their unique applications because of their small-size effects. A variety of anisotropic nanostructures such as nanoparticles [1], nanowires [2], and nanosheets [3] are usually preferable to bulk materials in technological applications. They have been thoroughly studied as potential building blocks for the fabrication of novel nanodevices. Among various metal chalcogenide semiconductors, copper(I) sulfide (Cu<sub>2</sub>S) has an energy bandgap of 1.21 eV that could be applied in optoelectronics and photocatalysis [4–6]. Cu<sub>2</sub>S nanomaterials are quite attractive because many of the proposed fabrication methods are inexpensive and lend themselves well to mass production [4–8]. Cu<sub>2</sub>S nanostructures, including nanocrystals, nanowires, and nanosheets, have aided in developing highly efficient photocatalysts for the environmental photocatalytic degradation of organic pollutants [6–8].

Meanwhile, chalcogenide semiconductors combined with noble metals like Au or Ag nanoparticles (NPs) have received massive attention; they have been extensively explored for their potential applications in the fields of surface-enhanced Raman scattering (SERS) [9–12] and photocatalysis [6,13,14]. The photocatalytic mechanism in noble metals–semiconductor composites has been discussed extensively [15,16]. The Schottky barrier at the interface has been proven to facilitate the charge separation and hence improve the photocatalytic efficiency [17]. On the other hand, SERS has been recognized as a powerful technique for the ultra-sensitive detection of a variety of chemical and biochemical molecules [18,19]. The SERS effect has been primarily attributed to the intensified electric field associated with the local surface plasmon resonance (LSPR) of metallic nanoparticles and electromagnetic (EM) enhancement. Previous studies demonstrated that Ag NPs feature greater advantages over Au and Cu NPs owing to their stronger plasmonic effect and

ease of synthesis [20]. The enhancement factor (EF) of the SERS signal can be up to  $10^3$ – $10^{14}$ , enabling single-molecule detection in some cases [21–23]. The extremely high enhancement signal has made SERS a very powerful tool to detect trace amounts of molecules adsorbed in the surface of noble metals [24].

Herein, we demonstrate a facile and environmentally friendly approach to synthesize  $\text{Cu}_2\text{S}$  nanosheets decorated with Ag NPs (Ag/ $\text{Cu}_2\text{S}$  nanosheets) by using a convenient galvanic reduction method. In the SEM nanostructure investigation, Ag NPs were preferentially deposited on the edge of  $\text{Cu}_2\text{S}$  nanosheets, where many activated sites led to the easy deposition of Ag NPs. Ordered Ag NPs are extremely attractive catalysts because of their significant catalytic activities [25], size- or shape-dependent optical properties [26], and promising chemical and biological sensing based on SERS and localized surface plasma resonance (LSPR) [16,27–29]. The results suggest that Ag/ $\text{Cu}_2\text{S}$  nanosheets have a high-performance SERS effect that can be applied in optoelectronic devices; furthermore, they show promising photocatalytic potential for new types of future applications.

## 2. Materials and Methods

### 2.1. Preparation of $\text{Cu}_2\text{S}$ Nanosheets

In a typical chemical experiment procedure, 8 mmol of sulfur powder ( $\geq 99.0\%$ , Sigma-Aldrich, St. Louis, MO, USA), 15 g of sodium hydroxide (NaOH,  $\geq 98\%$ , Sigma), 14 mL of ethylenediamine ( $\geq 99\%$ , Sigma), and 80  $\mu\text{L}$  of hydrazine (98%, Sigma) were sequentially dissolved in 80 mL of deionized (DI) water, and reaction temperature was controlled at 50 °C. A cleaned polycrystalline copper foil (Nanya corporation, Taipei, Taiwan) was used as the substrate to grow  $\text{Cu}_2\text{S}$  nanosheets, and it was placed in the solution for 30 s. The obtained black substrate was taken out and cleaned with isopropyl alcohol and DI water three times and finally stored under a vacuum.

### 2.2. Preparation of Ag/ $\text{Cu}_2\text{S}$ Nanosheets

Ag-NP-decorated  $\text{Cu}_2\text{S}$  nanosheets (Ag/ $\text{Cu}_2\text{S}$ ) were prepared via the galvanic reduction method. A 0.01 M silver nitrate ( $\text{AgNO}_3$ , Merck, Darmstadt, Germany) solution was prepared and heated at different temperatures (20, 30, and 40 °C). The black  $\text{Cu}_2\text{S}$  nanosheets were immersed into the  $\text{AgNO}_3$  solution for 10 s and then immediately removed from the solution. The Ag/ $\text{Cu}_2\text{S}$  nanosheets were thoroughly cleaned with isopropyl alcohol and DI water several times and finally preserved under a nitrogen atmosphere.

### 2.3. Characterizations

Several analytical techniques were used for the morphological characterization of the  $\text{Cu}_2\text{S}$  and Ag/ $\text{Cu}_2\text{S}$  nanosheets. A scanning electron microscope (SEM Quanta 200, FEI, Hillsboro, OR, USA) equipped with an energy-dispersive X-ray spectrometer was used to determine the morphologies and chemical composition of the  $\text{Cu}_2\text{S}$  and Ag/ $\text{Cu}_2\text{S}$  nanosheets. The high-resolution lattice images of the  $\text{Cu}_2\text{S}$  nanostructure were obtained using a transmission electron microscope (TEM JEM 2100, JEOL, Tokyo, Japan), operating at 200 keV. X-ray diffraction (XRD D2, Bruker, Karlsruhe, Germany) was used to understand the crystallography of the  $\text{Cu}_2\text{S}$  and Ag/ $\text{Cu}_2\text{S}$  nanosheets on the Cu foil and was recorded with a diffractometer using Cu  $K\alpha$  radiation at the rate of 0.02 per step. In order to investigate the process of electron transfer on the Ag/ $\text{Cu}_2\text{S}$  nanosheets, X-ray photoelectron spectroscopy (XPS, Thermo Scientific, Waltham, MA, USA) was used to analyze the Ag and Cu spectra at the interface between the Ag NP and  $\text{Cu}_2\text{S}$  nanosheets. A UniRAM-Raman spectrometer (ProTrusTech, Tainan, Taiwan) equipped with a 532 nm laser was used to record the SERS spectra of a rhodamine 6G (R6G, 99%, Merck) probe dropped over the prepared Ag/ $\text{Cu}_2\text{S}$  substrates. The photocatalytic activity of Ag/ $\text{Cu}_2\text{S}$  towards rhodamine B (RhB) degradation was evaluated under UV irradiation using a 200W HgXe arc lamp. The photodegradation experiments were performed by using Ag/ $\text{Cu}_2\text{S}$  films of  $1 \times 1 \text{ cm}^2$  area immersed in 6 mL of 10  $\mu\text{M}$  RhB (98%, Sigma) solution. UV-visible absorption spectra

of the RhB solution were recorded using a spectrophotometer (Evolution 60S, Thermo Scientific, Waltham, MA, USA).

### 3. Results and discussion

#### 3.1. Morphology and Structure of Ag/Cu<sub>2</sub>S Nanosheets

Figure 1a shows the SEM image of the nanosheets morphology of the Cu<sub>2</sub>S with an average diameter of around 5  $\mu$ m and thickness below 20 nm. The transmission-electron-microscopy (TEM) images shown in Figure S1 provide direct crystal information on the Cu<sub>2</sub>S nanosheets. Figure 1b–d shows the SEM images of Ag/Cu<sub>2</sub>S nanosheets grown in AgNO<sub>3</sub> solution at different temperatures of 20, 30, or 40  $^{\circ}$ C, respectively; these images indicate that the morphology of Ag NPs is dependent on the temperature of the galvanic AgNO<sub>3</sub> solution. As shown in Figure 1c, Ag NPs were preferentially located on the edge of the Cu<sub>2</sub>S nanosheets, which could be explained by the localization of the electrons on the edge of the Cu<sub>2</sub>S nanosheets. Lower ion diffusion can result in much smaller Ag clusters at a relatively low reaction temperature that decreases the decorating rate of Ag NPs on the edge of the Cu<sub>2</sub>S nanosheets. In contrast to low temperatures, Ag NPs are prone to be aggregated at relatively high reaction temperatures. After comparing the SEM images of Figure 1a–d to explore the optimal temperature value for fabricating high-quality Ag/Cu<sub>2</sub>S nanosheets, we found it to be 30  $^{\circ}$ C. The successful decoration of Ag NPs onto the surface of Cu<sub>2</sub>S nanosheets was also confirmed by the EDX elemental analysis as shown in Figure 1e. The inset SEM image of Figure 1e shows the high-quality and uniform Ag/Cu<sub>2</sub>S nanosheets of the existing 100 nm Ag NPs that were well-deposited on the edge of the Cu<sub>2</sub>S nanosheets. Moreover, the crystal structure of the Ag/Cu<sub>2</sub>S nanosheets was determined by X-ray diffraction. Figure 1f shows the typical XRD patterns of the undecorated Cu<sub>2</sub>S nanosheets and Ag/Cu<sub>2</sub>S nanosheets. All diffraction peaks could be ascribed to the orthorhombic crystal of Cu<sub>2</sub>S (JCPDS No. 23-0961) with lattice constants of  $a = 1.35$  nm,  $b = 2.73$  nm, and  $c = 1.19$  nm [8], apart from the three additional peaks ( $2\theta = 27.52^{\circ}$ ,  $43.32^{\circ}$ , and  $50.45^{\circ}$ ) corresponding to the Cu foil. Even though the peak intensity of the Ag NPs of the Ag/Cu<sub>2</sub>S nanosheets was lower than that of the Cu<sub>2</sub>S structures in the XRD patterns, the appearance of the peak of the Ag (111) diffraction plane is clear in Figure 1f, indicating that Ag NPs were successfully embedded in the interface of the Cu<sub>2</sub>S nanosheets.

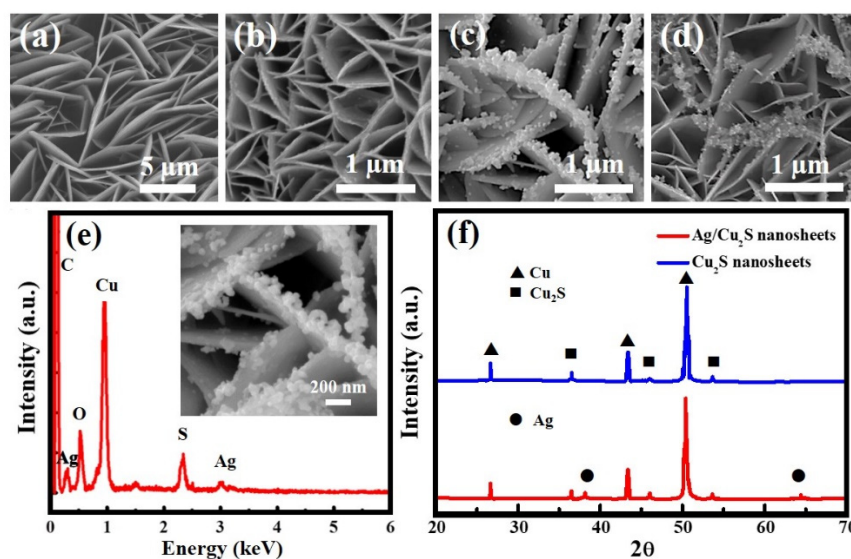


**Figure 1.** SEM images of (a) Cu<sub>2</sub>S nanosheets and Ag/Cu<sub>2</sub>S prepared at (b) 20  $^{\circ}$ C, (c) 30  $^{\circ}$ C, and (d) 40  $^{\circ}$ C. (e) EDX analysis of Ag/Cu<sub>2</sub>S nanosheets prepared at 30  $^{\circ}$ C. The inset SEM image reveals 100 nm Ag NPs were well deposited on the edge of 30  $^{\circ}$ C immersed Ag/Cu<sub>2</sub>S nanosheets. (f) XRD patterns of Cu<sub>2</sub>S nanosheets and Ag/Cu<sub>2</sub>S nanosheets prepared at 30  $^{\circ}$ C.

### 3.2. SERS Evaluation of Ag/Cu<sub>2</sub>S Nanosheets

Raman spectroscopy is a spectroscopic technique to observe vibrational, rotational, and other low-frequency modes in a system. Active SERS substrates can provide excellent sensitivity to measure the vibrational spectra of specific adsorbed molecules [9,10]. However, the intensity and reliability of SERS critically depend on the surface morphology and geometry of the nanostructured materials. The SERS performance of the Ag/Cu<sub>2</sub>S nanosheets was explored using R6G dye as a probe molecule, which is widely used in the field of SERS applications. As shown in Figure 2b, the Ag/Cu<sub>2</sub>S nanosheets obtained at 30 °C possess brilliant SERS performance in contrast to the poor SERS performance of the undecorated Cu<sub>2</sub>S nanosheets. Through four repeated experiments, we provide evidence that the results are reproducible. The reliability tests of SERS spectra, as shown in Figure S2, were collected in a 10<sup>-4</sup> M R6G dye solution by using repeated Ag/Cu<sub>2</sub>S nanosheets. Comparing data from the four repeated experiments, the results showed a slight shift in the SERS spectra (see Figure S2 in Supplementary Files).

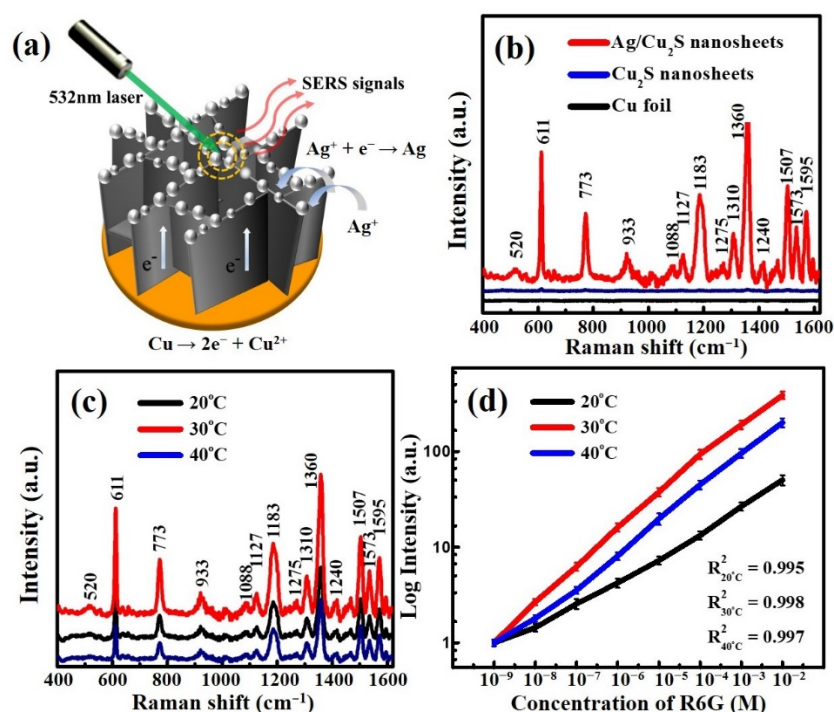


**Figure 2.** (a) Illustration of SERS sensing of Ag/Cu<sub>2</sub>S nanosheets for detection of rhodamine 6G (R6G) dye molecule. (b) SERS spectra of R6G dye adsorbed on three different substrates: Cu foil, Cu<sub>2</sub>S, and Ag/Cu<sub>2</sub>S nanosheets. (c) SERS spectra of R6G using Ag/Cu<sub>2</sub>S prepared at different temperatures of 20, 30, and 40 °C. (d) Linear correlation between the concentration of R6G and the intensity of characteristic SERS peak at different immersed temperatures of 20, 30, and 40 °C.

According to Figure 2c, Ag/Cu<sub>2</sub>S nanosheets prepared at 30 °C possess better SERS performance than those obtained at 20 and 40 °C, which can be attributed to the uniform distribution of the Ag NPs on the edge of the Cu<sub>2</sub>S nanosheets at 30 °C. As shown in Figure 2d, SERS intensity was accordingly decreased, while the concentration of the R6G dye molecule decreased. However, SERS signals still detected as low a concentration of the R6G dye molecule at 10<sup>-9</sup> M, as shown in Figure 2d, which presented a linear experimental relationship between SERS intensity and the concentration of the R6G dye molecule. The correlation refers to the straight-line relationships between 10<sup>-2</sup> and 10<sup>-9</sup> M, with a constant of proportionality that suggested that the number of adsorption sites with high Raman enhancement was large enough to accommodate a considerable range of sample concentrations. The results showed that there was a good linear correlation

between characteristic SERS peak intensity and R6G concentration with an  $R^2$  of around 99.5% to 99.8%.

### 3.3. Photocatalytic Activity of Ag/Cu<sub>2</sub>S Nanosheets

The photocatalytic activity of Cu<sub>2</sub>S and Ag/Cu<sub>2</sub>S nanosheets was investigated using RhB dye, and the process was monitored by UV-visible spectroscopy as shown in Figure 3a,b. A profound decrease in the absorbance of RhB was observed when the Cu<sub>2</sub>S nanosheets were decorated with Ag NPs at 30 °C. The improved photocatalytic activity can be attributed to the enhanced electron-hole ( $e^-$ - $h^+$ ) separation resulting from the Schottky barrier at the interface of the Ag/Cu<sub>2</sub>S nanosheet heterojunction, as illustrated by the inset in Figure 3b [15,16]. Therefore, Ag NPs can act as electron sinks, thereby reducing the recombination of photoinduced electrons and holes, and can prolong the lifetime of the ( $e^-$ - $h^+$ ) pairs. The photodegradation efficiency ( $\eta$ ) of the RhB dye molecule was calculated based on the absorbance for a period of 12 h of irradiation divided by the initial absorbance of the pollutant solution. Figure 3c demonstrates that the efficiency ( $\eta$ ) of the RhB photodegradation using the Ag/Cu<sub>2</sub>S nanosheets and undecorated Cu<sub>2</sub>S nanosheets was 90.3 and 31.3, respectively. Interestingly, the photocatalytic activity of the Ag/Cu<sub>2</sub>S nanosheets surpassed that of the Cu<sub>2</sub>S nanowires in our previous work [8]. Figure 3d shows that the photocatalytic degradation of the RhB dye followed a pseudo-first-order reaction according to the Langmuir–Hinshelwood mechanism [30,31], applying Equation (1):

$$\ln C = \ln C_0 - kt \quad (1)$$

where  $C_0$  and  $C$  are the initial concentration and concentration at a particular time, respectively,  $t$  is irradiation time, and  $k$  is the photocatalytic degradation rate constant. The calculated photocatalytic rate constants of Ag/Cu<sub>2</sub>S nanosheets, undecorated Cu<sub>2</sub>S nanosheets, and Cu<sub>2</sub>S nanowires (our previous work) were found to be 0.242, 0.029, and 0.077, respectively. These findings demonstrate that the Ag/Cu<sub>2</sub>S nanosheets had an enhancement that was 10 times larger than that of the undecorated Cu<sub>2</sub>S nanosheets.

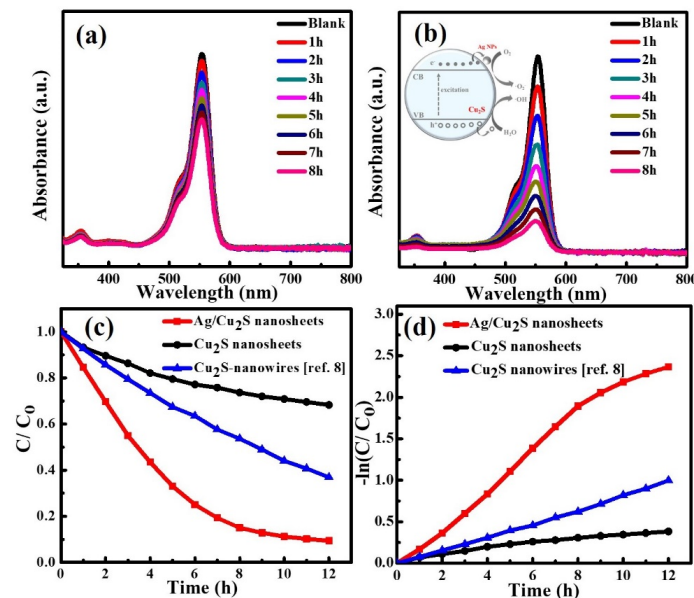


**Figure 3.** UV-visible absorption of RhB dye during the photodegradation process using (a) Cu<sub>2</sub>S and (b) Ag/Cu<sub>2</sub>S nanosheets. The inset illustrates the electron transfer process in Ag/Cu<sub>2</sub>S under light irradiation. (c) Relative change in concentration of the RhB dye during the photodegradation over different photocatalysts. (d) Kinetics of photodegradation and apparent rate constant ( $k$ ) using three different catalysts. Photodegradation results of Cu<sub>2</sub>S nanowires were mentioned in our previous report [8].

The additional Ag NP decoration process could decrease the band gap of Cu<sub>2</sub>S nanosheets, and thus favor electron transfers from the valence band to the conduction band. This might lead to an increase in the formation rate of oxidative species, such as the hydroxyl radicals ( $\bullet\text{OH}$ ), as compared to that of the Cu<sub>2</sub>S under the same experimental conditions. Therefore, in order to get insight into the electronic state in the Ag/Cu<sub>2</sub>S nanosheets, XPS analysis was carried out and the results are shown in Figure 4. Figure 4a shows the Cu 2p<sub>2/3</sub> peak of the XPS spectrum of the Ag/Cu<sub>2</sub>S nanosheets that was broader than that of the undecorated Cu<sub>2</sub>S nanosheets, and consequently right-shifted to the higher-energy region by 0.2 eV. Furthermore, the Ag 3d<sub>5/2</sub> peak of the XPS spectrum of the Ag/Cu<sub>2</sub>S nanosheets was left-shifted toward the lower-energy region by 0.4 eV, as shown in Figure 4b. The contrasting shifts of binding energy provide direct evidence for the electron withdrawal of Ag NPs from the neighboring Cu<sub>2</sub>S nanosheets.

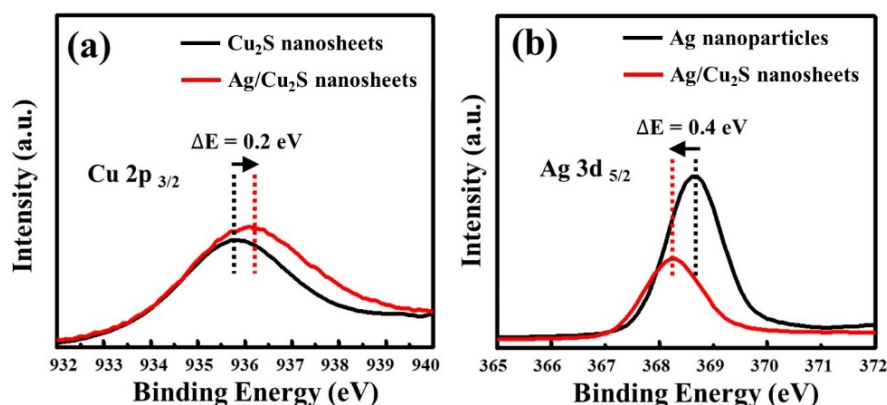


**Figure 4.** High resolution XPS spectra of Cu<sub>2</sub>S, Ag NPs, and Ag/Cu<sub>2</sub>S nanosheets: (a) Cu 2p<sub>2/3</sub> and (b) Ag 3d<sub>5/2</sub>.

#### 4. Conclusions

In summary, we successfully demonstrated a facile, rapid, and practical approach to synthesize large-scale and uniform Cu<sub>2</sub>S nanosheets and Ag-NP-decorated Cu<sub>2</sub>S nanosheets that have had a size-directing functionality in the reaction process. SEM images indicated that Ag NPs were preferentially deposited on the edge of Cu<sub>2</sub>S nanosheets due to the localization of the electrons on the surface. Localized field amplification that occurred during the excitation of surface plasmons of Ag NPs placed on Cu<sub>2</sub>S nanosheets enhanced UV-visible absorption of the incident photons within the Cu<sub>2</sub>S nanosheet region near each Ag NP. XPS spectra also showed that the Ag NPs on Cu<sub>2</sub>S nanosheets induced a binding-energy shift relative to that of the undecorated Cu<sub>2</sub>S nanosheets. Results provided proof for the electron withdrawal of Ag NPs from the Cu<sub>2</sub>S nanosheets. Ag/Cu<sub>2</sub>S nanosheets that were developed as a new technology in this field tended to follow a superlinear function compared with the Cu<sub>2</sub>S nanosheets, which reacted more slowly in photocatalytic activity. We tested different multifunctionality indicators in various experiments, such as the SERS effect and photodegradation process. The incorporation of Ag NPs highly increased the photodegradation efficiency of the RhB dye molecule under UV irradiation during a 12 h period. The efficient interfacial electron transfers from the excited Cu<sub>2</sub>S nanosheets to the Ag NPs would enhance the photodegradation of the RhB dye molecule. Ag/Cu<sub>2</sub>S nanosheets could perform as a promising dual photocatalyst for SERS applications and future photocatalytic materials.

**Supplementary Materials:** The following are available online at <https://www.mdpi.com/article/10.3390/nano1102508/s1>, Figure S1: Structural characterizations of undecorated Cu<sub>2</sub>S nanosheets. (a) The top-view SEM image and (b) EDX analysis of Cu<sub>2</sub>S nanosheets. (c) TEM images of Cu<sub>2</sub>S nanosheets. (d) The selected area electron diffraction (SAED) patterns of Cu<sub>2</sub>S nanosheets. Figure S2: SERS spectra show the reliability of Ag/Cu<sub>2</sub>S nanosheets towards 10<sup>-4</sup> M R6G dye detection.

**Author Contributions:** Conceptualization, C.-Y.C. and S.-W.L.; methodology, O.N., J.-R.J. and C.-Y.C.; validation, O.N. and J.-R.J. formal analysis, O.N. and J.-R.J.; investigation, O.N. and J.-R.J.; resources, C.-Y.C. and S.-W.L.; data curation, O.N. and J.-R.J.; writing—original draft preparation, O.N., W.-S.C., J.-R.J. and C.-Y.C.; writing—review and editing, O.N., W.-S.C., J.-R.J. and C.-Y.C.; supervision, C.-Y.C.; project administration, C.-Y.C. and S.-W.L.; funding acquisition, C.-Y.C. and S.-W.L. All authors have read and agreed to the published version of the manuscript.

**Funding:** This work was funded by the Ministry of Science and Technology, Taiwan, and the foundation grant MOST 107-2112-M-110-013-MY3 and MOST 110-2112-M-110-017-MY2.

**Data Availability Statement:** Not applicable.

**Conflicts of Interest:** The authors declare no conflict of interest.

## References

1. Khan, I.; Saeed, K.; Khan, I. Nanoparticles: Properties, applications and toxicities. *Arabian J. Chem.* **2019**, *12*, 908–931. [[CrossRef](#)]
2. Li, M.; Zhao, Z.; Cheng, T.; Fortunelli, A.; Chen, C.-Y.; Yu, R.; Zhang, Q.; Gu, L.; Merinov, B.V.; Lin, Z.; et al. Ultrafine jagged platinum nanowires enable ultrahigh mass activity for the oxygen reduction reaction. *Science* **2016**, *354*, 1414. [[CrossRef](#)]
3. Wang, G.; Li, D.; Cheng, H.-C.; Li, Y.; Chen, C.-Y.; Yin, A.; Zhao, Z.; Lin, Z.; Wu, H.; He, Q.; et al. Wafer-scale growth of large arrays of perovskite microplate crystals for functional electronics and optoelectronics. *Sci. Adv.* **2015**, *1*, e1500613. [[CrossRef](#)]
4. Grozdanov, I.; Najdoski, M. Optical and Electrical Properties of Copper Sulfide Films of Variable Composition. *J. Solid State Chem.* **1995**, *114*, 469–475. [[CrossRef](#)]
5. Wu, Y.; Wadia, C.; Ma, W.; Sadler, B.; Alivisatos, A.P. Synthesis and Photovoltaic Application of Copper(I) Sulfide Nanocrystals. *Nano Lett.* **2008**, *8*, 2551–2555. [[CrossRef](#)]
6. Kudo, A.; Miseki, Y. Heterogeneous photocatalyst materials for water splitting. *Chem. Soc. Rev.* **2009**, *38*, 253–278. [[CrossRef](#)]
7. Kim, Y.; Park, K.Y.; Jang, D.M.; Song, Y.M.; Kim, H.S.; Cho, Y.J.; Myung, Y.; Park, J. Synthesis of Au–Cu<sub>2</sub>S Core–Shell Nanocrystals and Their Photocatalytic and Electrocatalytic Activity. *J. Phys. Chem. C* **2010**, *114*, 22141–22146. [[CrossRef](#)]
8. Chen, C.-Y.; Jiang, J.-R.; Chuang, W.-S.; Liu, M.-S.; Lee, S.-W. Development of Crystalline Cu<sub>2</sub>S Nanowires via a Direct Synthesis Process and Its Potential Applications. *Nanomaterials* **2020**, *10*, 399. [[CrossRef](#)]
9. Li, X.; Chen, G.; Yang, L.; Jin, Z.; Liu, J. Multifunctional Au-Coated TiO<sub>2</sub> Nanotube Arrays as Recyclable SERS Substrates for Multifold Organic Pollutants Detection. *Adv. Funct. Mater.* **2010**, *20*, 2815–2824. [[CrossRef](#)]
10. Wang, H.H.; Liu, C.Y.; Wu, S.B.; Liu, N.W.; Peng, C.Y.; Chan, T.H.; Hsu, C.F.; Wang, J.K.; Wang, Y.L. Highly Raman-Enhancing Substrates Based on Silver Nanoparticle Arrays with Tunable Sub-10 nm Gaps. *Adv. Mater.* **2006**, *18*, 491–495. [[CrossRef](#)]
11. Tang, H.; Meng, G.; Huang, Q.; Zhang, Z.; Huang, Z.; Zhu, C. Arrays of Cone-Shaped ZnO Nanorods Decorated with Ag Nanoparticles as 3D Surface-Enhanced Raman Scattering Substrates for Rapid Detection of Trace Polychlorinated Biphenyls. *Adv. Funct. Mater.* **2012**, *22*, 218–224. [[CrossRef](#)]
12. D’Amato, C.A.; Giovannetti, R.; Zannotti, M.; Rommozzi, E.; Ferraro, S.; Seghetti, C.; Minicucci, M.; Gunnella, R.; Di Cicco, A. Enhancement of visible-light photoactivity by polypropylene coated plasmonic Au/TiO<sub>2</sub> for dye degradation in water solution. *Appl. Surface Sci.* **2018**, *441*, 575–587. [[CrossRef](#)]
13. Deng, Q.; Duan, X.; Ng, D.H.L.; Tang, H.; Yang, Y.; Kong, M.; Wu, Z.; Cai, W.; Wang, G. Ag Nanoparticle Decorated Nanoporous ZnO Microrods and Their Enhanced Photocatalytic Activities. *ACS Appl. Mater. Interfaces* **2012**, *4*, 6030–6037. [[CrossRef](#)]
14. Sarina, S.; Waclawik, E.R.; Zhu, H. Photocatalysis on supported gold and silver nanoparticles under ultraviolet and visible light irradiation. *Green Chem.* **2013**, *15*, 1814–1833. [[CrossRef](#)]
15. Li, X.Z.; Li, F.B. Study of Au/Au<sup>3+</sup>-TiO<sub>2</sub> Photocatalysts toward Visible Photooxidation for Water and Wastewater Treatment. *Environ. Sci. Technol.* **2001**, *35*, 2381–2387. [[CrossRef](#)]
16. Haes, A.J.; Van Duyne, R.P. A Nanoscale Optical Biosensor: Sensitivity and Selectivity of an Approach Based on the Localized Surface Plasmon Resonance Spectroscopy of Triangular Silver Nanoparticles. *J. Am. Chem. Soc.* **2002**, *124*, 10596–10604. [[CrossRef](#)] [[PubMed](#)]
17. Kumar, S.; Lodhi, D.K.; Singh, J.P. Highly sensitive multifunctional recyclable Ag–TiO<sub>2</sub> nanorod SERS substrates for photocatalytic degradation and detection of dye molecules. *RSC Adv.* **2016**, *6*, 45120–45126. [[CrossRef](#)]
18. Nie, S.; Emory, S.R. Probing Single Molecules and Single Nanoparticles by Surface-Enhanced Raman Scattering. *Science* **1997**, *275*, 1102. [[CrossRef](#)]
19. Tang, H.; Zhu, C.; Meng, G.; Wu, N. Review—Surface-Enhanced Raman Scattering Sensors for Food Safety and Environmental Monitoring. *J. Electrochem. Soc.* **2018**, *165*, B3098–B3118. [[CrossRef](#)]

20. Lin, J.; Guan, G.; Yang, W.; Fu, H. The enhanced Raman scattering of Ag nanoparticles decorated on the carbon nanotube via a simple manipulation. *Opt. Mater.* **2019**, *95*, 109258. [[CrossRef](#)]
21. Dick, L.A.; Haes, A.J.; Van Duyne, R.P. Distance and Orientation Dependence of Heterogeneous Electron Transfer: A Surface-Enhanced Resonance Raman Scattering Study of Cytochrome c Bound to Carboxylic Acid Terminated Alkanethiols Adsorbed on Silver Electrodes. *J. Phys. Chem. B* **2000**, *104*, 11752–11762. [[CrossRef](#)]
22. Li, C.; Yu, J.; Xu, S.; Jiang, S.; Xiu, X.; Chen, C.; Liu, A.; Wu, T.; Man, B.; Zhang, C. Constructing 3D and Flexible Plasmonic Structure for High-Performance SERS Application. *Adv. Mater. Technol.* **2018**, *3*, 1800174. [[CrossRef](#)]
23. Huang, Z.; Meng, G.; Huang, Q.; Yang, Y.; Zhu, C.; Tang, C. Improved SERS Performance from Au Nanopillar Arrays by Abridging the Pillar Tip Spacing by Ag Sputtering. *Adv. Mater.* **2010**, *22*, 4136–4139. [[CrossRef](#)]
24. Kwon, K.; Lee, K.Y.; Lee, Y.W.; Kim, M.; Heo, J.; Ahn, S.J.; Han, S.W. Controlled Synthesis of Icosahedral Gold Nanoparticles and Their Surface-Enhanced Raman Scattering Property. *J. Phys. Chem. C* **2007**, *111*, 1161–1165. [[CrossRef](#)]
25. Roucoux, A.; Schulz, J.; Patin, H. Reduced Transition Metal Colloids: A Novel Family of Reusable Catalysts? *Chem. Rev.* **2002**, *102*, 3757–3778. [[CrossRef](#)] [[PubMed](#)]
26. Wiley, B.J.; Chen, Y.; McLellan, J.M.; Xiong, Y.; Li, Z.-Y.; Ginger, D.; Xia, Y. Synthesis and Optical Properties of Silver Nanobars and Nanorice. *Nano Lett.* **2007**, *7*, 1032–1036. [[CrossRef](#)] [[PubMed](#)]
27. Willets, K.A.; Van Duyne, R.P. Localized Surface Plasmon Resonance Spectroscopy and Sensing. *Ann. Rev. Phys. Chem.* **2007**, *58*, 267–297. [[CrossRef](#)]
28. Unser, S.; Bruzas, I.; He, J.; Sagle, L. Localized Surface Plasmon Resonance Biosensing: Current Challenges and Approaches. *Sensors* **2015**, *15*, 15684–15716. [[CrossRef](#)]
29. Xu, S.; Man, B.; Jiang, S.; Wang, J.; Wei, J.; Xu, S.; Liu, H.; Gao, S.; Liu, H.; Li, Z.; et al. Graphene/Cu Nanoparticle Hybrids Fabricated by Chemical Vapor Deposition As Surface-Enhanced Raman Scattering Substrate for Label-Free Detection of Adenosine. *ACS Appl. Mater. Interfaces* **2015**, *7*, 10977–10987. [[CrossRef](#)]
30. Chen, C.-Y.; Lin, T.-C.; Chuang, W.-S.; Chang, J.-K.; Lee, S.-W. Germanium-assisted growth of titanium dioxide nanowires for enhanced photocatalytic and electron emission performance. *Appl. Surf. Sci.* **2020**, *530*, 147204. [[CrossRef](#)]
31. Malato, S.; Fernández-Ibáñez, P.; Maldonado, M.I.; Blanco, J.; Gernjak, W. Decontamination and disinfection of water by solar photocatalysis: Recent overview and trends. *Catal. Today* **2009**, *147*, 1–59. [[CrossRef](#)]